THE ASTROPHYSICAL JOURNAL, 327:66–81, 1988 April 1

COOLING FLOWS AND THE STABILITY OF RADIO JETS

NOAM SOKER AND CRAIG L. SARAZIN
Department of Astronomy, University of Virginia
Received 1987 April 1; accepted 1987 September 25

ABSTRACT

Recent X-ray observations of elliptical galaxies show that they contain significant quantities of hot gas, which probably form cooling flows. This is particularly true of central dominant cluster galaxies. Radio galaxies are generally associated with elliptical galaxies. We consider the effects which these cooling flows can have on the propagation of radio jets. Under many conditions, these cooling flows will have sonic radii at which the flows become transonic. We show that the pressure and temperature of the cooling flow gas will drop precipitously with decreasing radius just inside of the sonic radius. When an outwardly propagating radio jet encounters this pressure "wall," we show that it can be disrupted. We also find that a radio jet can be deflected if it encounters the sonic region of the cooling flow at an oblique angle. The cooling flow sonic radii occur on much smaller scales (100–1000 pc) than the sizes of the radio sources associated with elliptical galaxies. We conclude, therefore, that the radio jets are not disrupted at cooling flow sonic radii in most cases. However, we also discuss several specific radio sources in which the small-scale radio structure is consistent with jet disruption at the cooling flow sonic radius. For the cases in which the jets are not disrupted, we suggest that either the radio jets are slow and heavy ($v \ll c$) on these scales, or that very little of the material in the cooling flows reaches the sonic radius.

Subject headings: galaxies: interstellar matter — galaxies: jets — radio sources: general

I. INTRODUCTION

It is well known that strong, extended extragalactic radio sources are generally associated with elliptical galaxies. The energy which is observed in the large-scale radio emission is believed to ultimately arise from the nucleus of the galaxies and is delivered to the large-scale radio lobes by jets (see, for example, Miley 1980). In addition to the radio sources associated with normal large elliptical galaxies, distorted radio sources, called wide-angle tail (WAT) sources, are found to be associated with central dominant cluster galaxies.

X-ray and optical observations indicate that large amounts of gas are cooling at and flowing into the centers of clusters of galaxies (see the reviews by Fabian *et al.* 1984 and Sarazin 1986*a*). In every case observed so far, a central dominant cluster galaxy is found at the center of the cooling flow. Typically, these cluster cooling flows have cooling rates of $\dot{M} \approx 100\ M_\odot\ \mathrm{yr}^{-1}$ (Stewart *et al.* 1984; Fabian, Nulsen, and Canizares 1984).[1]

Recently, X-ray observations have shown that normal elliptical galaxies also contain large quantities of hot gas (Forman, Jones, and Tucker 1985; Trinchieri and Fabbiano 1985). There is considerable evidence that this gas also forms cooling flows (White and Chevalier 1984; Nulsen, Stewart, and Fabian 1984; Fabian 1987; Sarazin 1986*b*; Canizares, Fabbiano, and Trinchieri 1987; Sarazin and White 1987), with smaller cooling rates of $\dot{M} \approx 1\ M_\odot\ \mathrm{yr}^{-1}$.

This suggests that the interstellar medium of elliptical galaxies, whether cluster central or more isolated, consists of hot gas ($T \approx 10^7$ K) in the form of a cooling inflow. These cooling flows provide a unique physical environment for radio galaxies. One aspect of this environment is the presence of rather high interstellar gas pressures ($P/k \approx 10^6\ \mathrm{cm}^{-3}$ K), which may help to confine radio sources. In the outer parts of the cooling flow, the gas pressure increases slowly inward. If these cooling inflows continue into the centers of the elliptical galaxies, then the inflow will tend to become supersonic within a "sonic radius." In § II, we will show that the gas pressure drops very rapidly with decreasing radius within the sonic radius.

Thus, a radio jet propagating out from the nucleus of an elliptical galaxy will encounter a point at which the ambient gas pressure increases very rapidly. In this paper, we consider what happens to radio jets which run into such a pressure "wall." In § II, we calculate the pressure variation within the sonic radius of a cooling flow. In § III, we give a semi-analytical calculation of the stability of a jet which encounters a rapidly increasing pressure gradient. In § IV, we show the results of numerical hydrodynamic simulations which test the results of the analytic calculations. We also consider the case where the jet encounters the sonic region at an oblique angle, and we suggest that this may provide an explanation for jets which are bent on small scales. In § V, these results are applied to the radio sources associated with central dominant cluster galaxies (WATs) and with more normal elliptical galaxies. Recently, Sumi *et al.* (1988) have discussed the structure of the radio source in A2029 and have suggested that it is due to the cooling flow sonic radius.

Because the results of this paper are somewhat negative, we should point out that there are many other ways in which cooling flows can influence radio sources. Here are several examples. First, cooling inflows could provide the fuel to power the central engines of radio sources (Fabbiano *et al.* 1987). Second, as suggested by Begelman (1986), accretion from a cooling flow may lead to the formation of radio jets in a galactic nucleus; this might explain why radio sources are associated with elliptical galaxies. Third,

[1] All comparisons to observations in this paper assume a Hubble constant $H_0 = 50\ \mathrm{km\ s}^{-1}\ \mathrm{Mpc}^{-1}$ and $q_0 = 0$.

the cooling gas might form an accretion shock near the galaxy center; this might disrupt the jets in a similar fashion to the pressure wall near the sonic radius. Fourth, if jets survive the pressure wall at the sonic radius, they might be affected by the more gradually decreasing pressure in the outer parts of the cooling flow (Sumi and Smarr 1984). Fifth, radio jets might be disrupted at the transition region between the intragalactic cooling flow gas and the surrounding intergalactic or intracluster medium. There will probably be a considerable velocity shear in this layer. Finally, the gas in cooling flows is thermally unstable, and clumping may affect the propagation of jets (Burns *et al.* 1986).

II. COOLING FLOWS AND SONIC RADII

We will consider cooling flows onto central dominant galaxies in clusters and onto more isolated normal elliptical galaxies. The cluster cooling flows typically have cooling rates of $\dot{M} \approx 10^2\ M_\odot\ \mathrm{yr}^{-1}$ (Stewart *et al.* 1984; Fabian *et al.* 1984). The source of both the mass and enthalpy in a cluster cooling flow is the intracluster medium. In the cooling flows in normal elliptical galaxies, the source of the inflowing gas is probably mass loss by stars in the galaxy. Consistent with this suggestion, the individual galaxy cooling flows have steeper gas density distributions, with $\rho \approx r^{-3/2}$ in individual elliptical galaxies and $\rho \approx r^{-1}$ in clusters. The cooling rates in individual large elliptical galaxies are $\dot{M} \approx 10^0\ M_\odot\ \mathrm{yr}^{-1}$ (Forman, Jones, and Tucker 1985; Trinchieri and Fabbiano 1985; Sarazin 1986*b*; Canizares, Fabbiano, and Trinchieri 1987).

If this cooling inflow were spherically symmetric and homogeneous, then continuity would generally require that the flow pass through a sonic radius at which the inflow velocity increases through the sound speed. This occurs because the flows generally accelerate inward, and cooling of the gas lowers its sound speed. However, there are several reasons why this may not actually occur in real cooling flows. First, the infalling gas may have enough angular momentum to cause the flow to stagnate before becoming transonic. Second, cooling gas is very thermally unstable for $T \gtrsim 10^5$ K. As a result, the flow is very likely to be inhomogeneous. Thermally instabilities may effectively remove gas from the inflow. Since the coolest gas drops out of the flow most rapidly, the remaining gas may well remain hot. The resulting decrease in the inflow rate and increase in the sound speed can cause the inflow to remain subsonic all the way into the center of the galaxy (White and Sarazin 1987*a*, *b*, *c*). Unfortunately, it is difficult to check for the existence of sonic radii in cooling flows experimentally, because the expected sonic radii for either cluster or individual galaxy cooling flows are too small to be resolved by the existing X-ray observations. In what follows, we will assume that cooling flows generally possess sonic radii; we note that the numerical models of White and Sarazin (1986*c*) which include thermal instabilities still possess sonic radii, although they are considerably smaller than in homogeneous cooling flow models. The effect of the sonic radius on radio jets may actually be used to test whether such sonic radii do indeed exist.

One important feature of cooling flows with sonic radii is that the entropy and pressure of the gas drop rapidly just within the sonic radius. Figure 1 shows the variation of the gas pressure in two simple numerical models for cooling flows; the model for an individual elliptical galaxy is taken from Sarazin and White (1987), while the cluster cooling flow models uses the numerical code developed by White and Sarazin (1987*c*). In general, the pressure drops to essentially zero at a critical radius $r_c \approx 0.7 r_s$, where r_s is the sonic radius of the cooling flow. There are two reasons for this drop in the pressure. First, within the sonic radius the inflow is

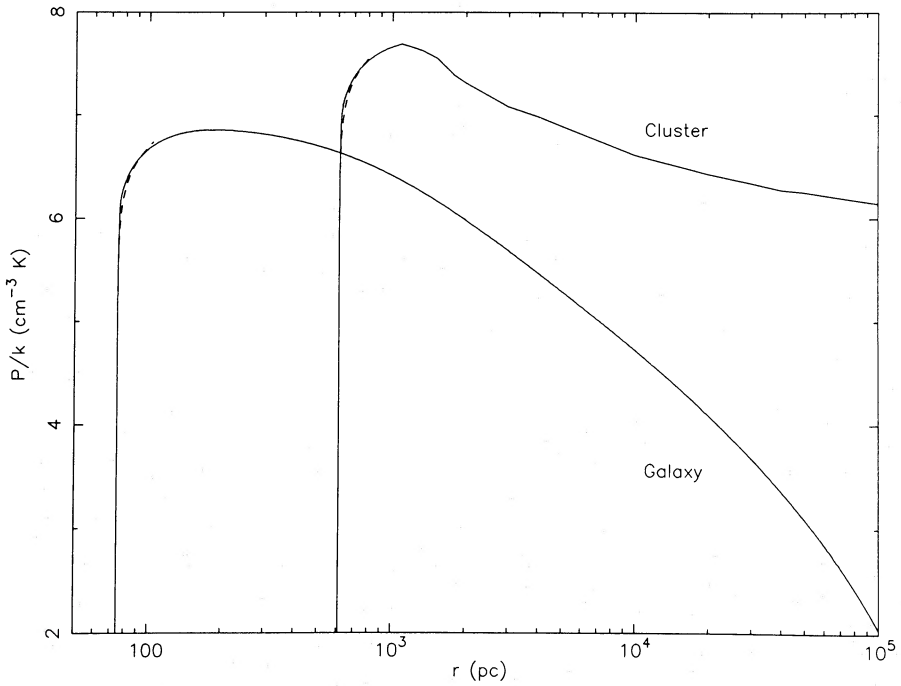

FIG. 1.—Pressure vs. radius in cooling flow models for clusters and for individual elliptical galaxies. The pressure (actually $P/k = nT$) is plotted as a function of the radius (in parsecs). Solid curve labeled "Galaxy" is model 18 from Sarazin and White (1987) for an individual elliptical with an optical luminosity of $L_B = 10^{11}\ L_\odot$. Solid curve labeled "Cluster" is for a cluster cooling flow with $\dot{M} = 300\ M_\odot\ \mathrm{yr}^{-1}$ and no star formation, from White and Sarazin (1987). The barely distinguishable dashed lines are the semi-analytic approximation (eq. [8]).

supersonic, and conditions downstream can have no influence on the properties of the gas at the sonic radius. Thus, the drop in pressure doesn't lower the gas density and pressure or alter the position at the sonic radius. Second, at the sonic radius in a cooling flow, the cooling time and inflow time are comparable. At the temperatures of interest ($T \approx 10^6$–10^7 K), as the temperature decreases cooling accelerates rapidly, and the cooling time gets much shorter. On the other hand, within the sonic radius, the gas velocity is roughly constant, so the flow time does not decrease rapidly. As a result, the gas cools almost completely before it has flowed in very far from the sonic radius. (We note, however, that the *total* pressure may not show such an extreme drop because the magnetic pressure doesn't decrease with decreasing temperature [Soker and Sarazin 1987].)

We now give a number of very simple arguments which establish roughly the location of the sonic radius r_s, and the values of the pressure at the sonic radius P_s and the maximum cooling flow pressure P_m (which usually occurs just outside the sonic radius). We will also derive a relatively simple approximate formula for the variation of the pressure in the region just within the sonic radius where it increases very rapidly with increasing radius. We will ignore sources of either mass or of heating of the inflowing gas. In the case of cluster cooling flows, ignoring sources of gas is obviously justified since the sonic radius is much smaller than the core radius of the cluster. In the case of an individual galaxy, the sonic radius is typically much smaller than the effective radius of the galaxy, so nearly all of the stars (which provide the mass and heating of the gas) are well outside of the sonic radius. We will assume that the cooling flow is spherical, and in steady state. The equations for such a flow have been given by White and Sarazin (1987*a*) and Sarazin and White (1987). Following White and Sarazin (1987*a*), we will assume that, if thermal instabilities are effective, they remove gas from the inflow at a rate $\dot{\rho} = -q\rho/t_c$, where t_c is the adiabatic cooling time. If $q = 0$, then the situation reduces to that of a homogeneous cooling flow. The cooling rate per unit volume in the gas is given by $\rho^2\Lambda(T)$, where we will assume that the cooling function Λ is a power-law function of the temperature $\Lambda \propto T^{\alpha}$; we note that $\alpha \approx -0.6$ crudely approximates the cooling rate for 10^5 K $\lesssim T \lesssim 3 \times 10^7$ K.

Let P_s, ρ_s, T_s, v_s, $\dot{M}_s$, and Λ_s be the values of the gas pressure, density, temperature, inflow velocity, mass inflow rate, and cooling function at the sonic radius. Three conditions can be used to derive the position of the sonic radius and the pressure at the sonic radius as a function of $\dot{M}_s$ and T_s. First, by definition, the flow speed v_s at the sonic radius is the sound speed of the gas, so that $v_s = (5kT_s/3\mu m_p)^{1/2}$, where μ is the mean mass per particle in the gas. Second, as long as pressure forces in the flow are significant compared to gravitational forces, the flow time will be approximately the cooling time in the gas $t_{\rm flow} \equiv (r_s/v_s) \approx t_{\rm cool}$. Finally, the mass inflow rate is obviously just $\dot{M}_s = 4\pi\rho_s v_s r_s^2$. These conditions imply that

$$r_s \approx \frac{3\dot{M}_s\Lambda_s}{100\pi}\left(\frac{kT_s}{\mu m_p}\right)^{-2} \approx 0.4 \text{ kpc}\left(\frac{\dot{M}_s}{1\ M_\odot\ \text{yr}^{-1}}\right)\left(\frac{T_s}{10^6\ \text{K}}\right)^{-2.6} . \tag{1}$$

This equation is derived in considerably more detail in Sarazin (1986*b*), where the value of the numerical coefficient is justified. From equations (1) and our assumptions, it is easy to show that

$$P_s \approx \left(\frac{3}{5}\right)^{1/2}\frac{25}{3\Lambda_s r_s}\left(\frac{kT_s}{\mu m_p}\right)^{2.5} \approx 1 \times 10^5 k\left(\frac{T_s}{10^6\ \text{K}}\right)^{3.1}\left(\frac{r_s}{\text{kpc}}\right)^{-1} . \tag{2}$$

This equation can also be written as

$$P_s \approx 3 \times 10^4 k\left(\frac{\dot{M}_s}{1\ M_\odot\ \text{yr}^{-1}}\right)^{1.19}\left(\frac{r_s}{\text{kpc}}\right)^{-2.19} . \tag{3}$$

Note that equation (3) and the second version of equation (2) actually give the value for $P_s/k \equiv nT$. The temperature variations in the numerical forms of equations (1)–(3) assume that the cooling function varies as $\Lambda \propto T^{-0.6}$. The numerical forms of equations (1)–(3) have been compared to the elliptical galaxy cooling flow solutions of Sarazin and White (1987) and the cluster cooling flow solutions of White and Sarazin (1987*c*), and agree reasonably (within 40% for eqs. [1] and [2], and 60% for eq. [3]) in all of the cases which could be checked. The maximum value of the pressure P_m, which generally occurs just outside the sonic radius, is $P_m \approx 1.4P_s$ (to within 20%) in all of the models checked.

We now derive a simple approximation for the radial variation of the pressure in the region within the sonic radius, where the pressure is increasing rapidly with increasing radius. Inside of the sonic radius, the inflow is supersonic; we will assume that it is very supersonic $v^2 \gg P/\rho$ in the region where the pressure is increasing rapidly. Then, the kinetic plus potential energy in the inflow is conserved $v^2/2 + \phi(r) \approx$ constant, where $\phi(r)$ is the gravitational potential of the galaxy. Typically, the inflow velocity at the sonic radius is comparable to the velocity dispersion of the galaxy. The pressure drops very rapidly (Fig. 1), so that the potential probably does not change very rapidly in this region. This, we expect the inflow velocity is roughly constant, $v \approx v_c$.

Now, White and Sarazin (1987*a*) show that $\dot{M} \propto S^{3q/5}$ holds quite generally in a cooling flow, where

$$S \equiv \left(\frac{P}{P_s}\right)\left(\frac{\rho}{\rho_s}\right)^{-5/3} \tag{4}$$

is a function of the entropy in the gas. Then, the pressure varies as

$$\left(\frac{P}{P_s}\right) = S^{1+q}\left(\frac{v_c}{v_s}\right)^{-5/3}\left(\frac{r}{r_s}\right)^{-10/3} . \tag{5}$$

The energy equation for the flow can be solved to give

$$\frac{S^u}{u} = \left(\frac{2r_s\rho_s^2\Lambda_s}{3wP_s v_s}\right)\left(\frac{v_c}{v_s}\right)^{[-2(2+\alpha)]/3}\left(\frac{r}{r_s}\right)^w + C\,, \tag{6}$$

where $u \equiv (5 - 5\alpha - q - 2\alpha q)/5$, $w \equiv (1 - 4\alpha)/3$, and C is a constant of integration.

We now substitute typical numerical values into equation (6). As mentioned before, $\alpha \approx -0.6$ roughly fits the cooling function for temperatures in the range 10^5 K $\lesssim T \lesssim 3 \times 10^7$ K, which covers most of the region of interest. Then, $w \approx 1.13$ and $2(2 + \alpha)/3 \approx 0.93$. White and Sarazin (1987*a*) argue that the rate of growth of thermal instabilities is bounded by $0 \leq q \lesssim 2 - \alpha$, which implies that $1.60 \lesssim u \lesssim 1.70$. Because of the very weak dependence of u on q, we will take $u = 1.65$ in all following work. From numerical solutions for cooling flows (White and Sarazin 1987*a*; Sarazin and White 1987), one finds that $(v_s/v_c) \approx 0.7$. The previous equations imply that $(2r_s\rho_s^2\Lambda_s/3P_s v_s) \approx 10/3$. Now, at $r = r_s$, $S = 1$ by definition. Applying this condition to equation (6) yields $C \approx -1.5$. In equation (6), the combination of a negative value of C with positive values of u and w implies that the entropy and pressure go to zero at a finite radius r_c, as we noted at the beginning of this section. Substituting these results into equation (6) and setting $S = 0$ gives

$$r_c \approx 0.74 r_s\,, \tag{7}$$

which agrees reasonably with the results of the numerical models. The pressure is then found to vary roughly as

$$\frac{P}{P_s} \approx \left\{2.5\left[\left(\frac{r}{r_c}\right)^{1.13} - 1\right]\right\}^{(1+q)/1.65} \approx \left[2.85\left(\frac{r - r_c}{r_c}\right)\right]^{(1+q)/1.65} \tag{8}$$

for $r \approx r_c$. The second expression follows from the expansion of the first expression about $r = r_c$ and is accurate because of the low power of 1.13 in the first expression. The pressures given by equation (8) for the values of r_c and P_s for the two models in Figure 1 are plotted as dashed curves for $r_c \leq r \leq r_s$ on that figure. Equation (8) agrees with the detailed models to within 30% over the range shown.

Equations (1), (2), (3), and (8) will be used to model the pressure variation in this region of the cooling flow and to compare to the observations of radio galaxies.

III. JET DISRUPTION AT THE COOLING FLOW SONIC RADIUS: ANALYTICAL APPROACH

In this section, we make an analytic estimate of the stability of a jet which encounters the rapidly increasing pressure in a cooling flow near the sonic radius. Our basic criterion is that if the jet becomes subsonic or even slightly supersonic (Mach number $M \lesssim 1$), the jet will become unstable. This criterion is supported by numerical simulations and by analytical perturbation analyses (Sumi and Smarr 1984; Payne and Cohn 1985). The latter paper shows that this criterion applies to pressure-confined jets which have lower densities than the ambient confining gas; arguments indicating that this is true of radio jets on the scales of interest here are given by O'Dea (1985). His arguments are based on observations of narrow-angle tail radio sources, but may be applied more generally if one assumes that these are merely typical radio galaxies which happen to be associated with rapidly moving cluster galaxies. In applying this criterion for instability, we will assume that the jet propagates freely (is freely expanding) from the nucleus out to the region of the sonic radius. We consider two alternatives for the behavior of the jet when it encounters the rapidly increasing pressure near the sonic radius. First, we consider the possibility that the jet is able to come into pressure equilibrium with the ambient gas through an adiabatic compression. Second, we study the instability of the jet when it cannot reach equilibrium adiabatically, and instead undergoes one or several shocks.

First, we consider the possibility that the jet is compressed adiabatically in the region of increasing pressure, and that the jet becomes confined by the ambient gas pressure. The relevant equations (mass conservation, the Bernoulli equation, and the equation of state) which connect the properties of the jet interior to the high pressure region (region 1) with its properties in the high pressure region (region 2) are

$$\rho_1 v_1 s_1 = \rho_2 v_2 s_2\,, \tag{9}$$

$$\frac{1}{2}v_1^2 + \frac{\gamma}{\gamma - 1}\frac{P_1}{\rho_1} = \frac{1}{2}v_2^2 + \frac{\gamma}{\gamma - 1}\frac{P_2}{\rho_2}\,, \tag{10}$$

$$P = K\rho^\gamma\,, \tag{11}$$

where P, ρ, v, and s are the pressure, density, velocity, and cross-sectional area of the jet, respectively. Also, γ is the adiabatic index, and K is a constant depending on the entropy.

We take the high-pressure region to be at the maximum pressure in the cooling flow, and so by our assumption of confinement, $P_2 = P_m$. From equations (10) and (11) one can show (Sumi and Smarr 1984) that

$$M_2^2 = \frac{2}{\gamma - 1}\left[\left(\frac{P_2}{P_1}\right)^{(1-\gamma)/\gamma} - 1\right] + \left(\frac{P_2}{P_1}\right)^{(1-\gamma)/\gamma} M_1^2\,, \tag{12}$$

where $M = v/(\gamma P/\rho)^{1/2}$ is the Mach number. The jet will stay supersonic, $M > 1$, as long as the following condition holds:

$$\frac{P_m}{P_1} < \left[\frac{2 + (\gamma - 1)M_1^2}{\gamma + 1}\right]^{\gamma/(\gamma-1)}\,. \tag{13}$$

According to our criterion for instability, the jet will become unstable for $M \lesssim 1$. We will therefore take equation (13) as one condition required to avoid disrupting the jet.

We assume that the jet was not confined and was expanding freely before entering the high pressure region of the cooling flow. Then, the jet pressure and Mach number vary as (Sanders 1983)

$$P_1 = P_o\left(\frac{r}{r_o}\right)^{-2\gamma}, \tag{14}$$

$$M_1 = M_o\left(\frac{r}{r_o}\right)^{\gamma-1}, \tag{15}$$

where the subscript o refers to some point near the origin of the jet and r is the distance from the source of the jet. We will take r_o to be the sonic radius of the jet itself, so that $M_o \equiv 1$. We will assume that the sonic radius of the cooling flow (typically at $r_s \approx 10^2$ pc) is well outside the sonic point of the jet (perhaps at $r_o \lesssim 1$ pc), so the Mach number at the cooling flow sonic radius is quite high, $M_1^2 \gg 2/(\gamma - 1)$. These results lead to

$$\frac{P_m}{P_o} < \left(\frac{\gamma - 1}{\gamma + 1} M_o^2\right)^{\gamma/(\gamma-1)}, \tag{16}$$

as our condition for maintaining the jet. For example, for $\gamma = 5/3$ we find $P_m < (3\rho_o v_o^2/160)$. This means that to maintain the jet under adiabatic compression in the high-pressure region, the maximum pressure of the ambient medium should not be higher than the ram pressure in the initial jet, multiplied by some constant. Condition (16) doesn't depend on the position of the sonic radius in the cooling flow, but only on the presence of a high-pressure region associated with it.

Alternatively, we now consider the case where the jet goes through a conical strong shock at $r \approx r_c$, just before reaching the sonic radius and the maximum pressure region. We will assume that after the shock the jet continues to expand adiabatically into the maximum pressure region. Let ϕ be the angle between the conical shock front and the incoming stream line, and let the subscripts 1 and 2 refer to quantities before and after the shock, respectively. Of course, the hydrodynamical equations (9)–(11) can also be applied before and after the shock. The postshock Mach number M_2 for an oblique shock is given by Landau and Lifshitz (1959). For a strong shock $M_1^2 \sin^2 \phi \gg 1$, the stability criterion $M_2 > 1$ implies

$$\frac{P_m}{P_o} < \Gamma_I^2 M_o^2\left(\frac{r_c}{r_o}\right)^{-2}, \tag{17}$$

where

$$\Gamma_I^2 = (2\gamma)^{-1/(\gamma-1)}(\gamma + 1)^{(1-2\gamma)/(\gamma-1)}[(\gamma - 1)^2 + 4\gamma \cos^2 \phi]^{\gamma/(\gamma-1)}(\sin \phi)^{-2/(\gamma-1)}. \tag{18}$$

From equations (16) and (17), we see that the jet is more likely to be disrupted if it passes through a conical shock rather than compressed adiabatically, as long as if the critical radius r_c of the cooling flow satisfies the condition

$$\frac{r_c}{r_o} > \Gamma_I\left(\frac{\gamma + 1}{\gamma - 1}\right)^{\gamma/[2(\gamma-1)]}. \tag{19}$$

In Figure 2, we give the values of r_c/r_o from equation (19) for $\gamma = 5/3$ and $\gamma = 4/3$ as a function of ϕ. For most applications we will assume that $(r_c/r_o) \gg 1$ and any shock which occurs is strong; then, the jet is more likely to be disrupted after passing through a shock.

As a result, we will now concentrate on the case where the jet goes through a shock when it hits the very steep pressure gradient just inside of the sonic radius in a cooling flow. Unfortunately, the stability condition (eq. [17]) depends on the angle of this shock ϕ. We will now make a crude estimate of the structure of this shock and of the angle ϕ. We make a number of assumptions in order to make the problem tractable analytically. In § IV, hydrodynamical simulations are used to test these assumptions. These assumptions are based on studies by Shapiro (1953) and Courant and Friedrichs (1948) of overexpanded jets, as well as results taken from underexpanded nozzle flow (Adamson and Nicholls 1959; Chang and Chow 1974). First, we assume that the shock is a conical one without a Mach disk, as is the case for high Mach number flow in underexpanded jets (Chang and Chow 1974) and as can be the case for overexpanded jets (Shapiro 1953). However, under certain conditions a Mach disk is also possible (Courant and Friedrichs 1948; Shapiro 1953; see also § IV below). A Mach disk will always make the jet less stable than a conical shock. Second, following Adamson and Nicholls (1959) we will assume that the average pressure behind the conical shock is equal to the ambient medium pressure. Our third assumption is that the shock starts when the ambient gas pressure equal to the jet pressure, and we will take the ambient gas pressure from the simple analytical model in the previous section in the limit of no mass loss from the cooling flow ($q = 0$).

Let D be the distance from the starting point of the conical shock to its vertex, along the symmetry axis of the jet, and let R_j the radius of the jet, so that $D = R_j/\tan \phi$. Then, equation (8) with q taken to be zero implies that

$$P_2 \approx P_1\left(\frac{r - r_c + D}{r - r_c}\right)^{0.61} \tag{20}$$

We have assumed that the jet has a pressure equal to the ambient pressure following the shock. If the jet pressure is even higher, the Mach number in the jet will be lower, and the jet will be even more unstable. After substituting for $(r - r_c)$ from equation (8), for P_1

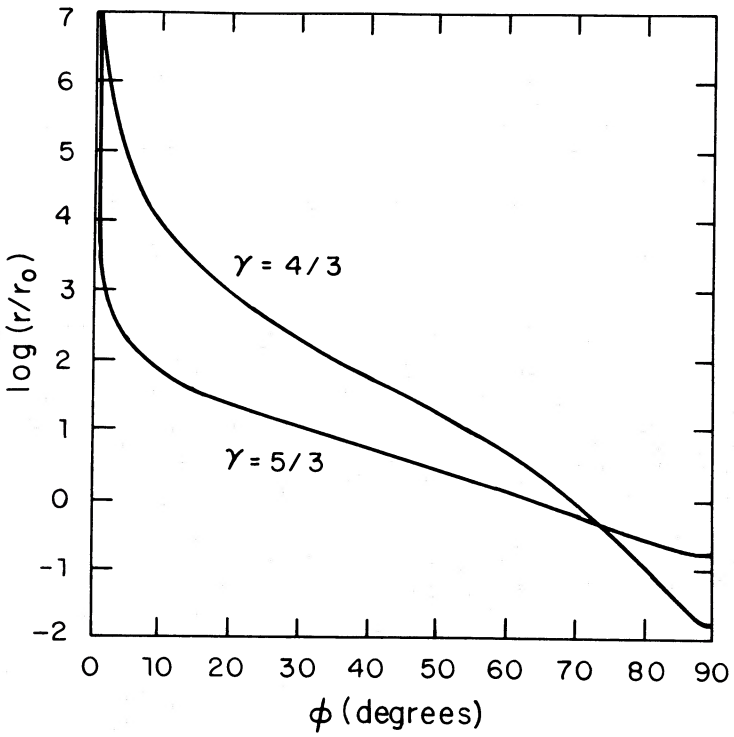

FIG. 2.—Common logarithm of (r_s/r_o) (the critical sonic radius for jet disruption over the initial radius of the jet) is plotted vs. conical shock angle ϕ from eq. (19) for $\gamma = 5/3$ and $\gamma = 4/3$.

from equation (14), for M_1 from equation (15), and after applying the strong oblique shock conditions to the pressure, we find

$$\left[\frac{2\gamma M_o^2 \sin^2\phi}{\gamma+1}\left(\frac{r_c}{r_o}\right)^{2(\gamma-1)}\right]^{1.65} \approx 1 + \frac{2.85}{\tan\phi}\left(\frac{R_j}{r_c}\right)\left[\left(\frac{P_s}{P_o}\right)\left(\frac{r_c}{r_o}\right)^{2\gamma}\right]^{1.65}. \tag{21}$$

For a strong shock, we can ignore the first term (unity) on the right-hand side of equation (21) for $r_c \gg r_o$ and obtain

$$\frac{r_c}{r_o} \approx \sin\phi\left(\frac{\tan\phi}{2.85}\right)^{0.30}\left(\frac{\gamma+1}{2\gamma}\right)^{1/2}\left(\frac{r_c}{R_j}\right)^{0.30}\left(\frac{P_o}{P_s}\right)^{1/2} M_o . \tag{22}$$

We now define $\beta \equiv R_j/r_c$ as the angular width of the jet; typically, $\beta \approx 0.1$ is observed. Now, the right-hand side in equation (22) depends only weakly on γ, so we will assume $\gamma = 5/3$ in the numerical values which follow. Then, equation (22) becomes

$$\frac{r_c}{r_o} \approx \sin\phi\left[\tan\phi\left(\frac{0.24}{\beta}\right)\right]^{0.30}\left(\frac{P_o}{P_s}\right)^{1/2} M_o . \tag{23}$$

The condition required for the stability of the jet (eq. [17]) can be rewritten as

$$\frac{r_c}{r_o} \lesssim \Gamma_I\left(\frac{P_o}{P_m}\right)^{1/2} M_o . \tag{24}$$

Considering the uncertainties in P_m, P_s, and R_j, we will take $P_m \approx 1.4P_s$ and $\beta \approx 0.1$. Obviously, the maximum value of the cooling flow sonic radius which allows a stable jet to exist must also satisfy equation (23). This requires that the angle ϕ satisfy $\Gamma_I \approx 1.54 \sin\phi\,(\tan\phi)^{0.30}$, which has the solution $\Gamma_I \approx 0.95$ or $\phi \approx 40°$, with a very weak dependence on γ. The final version of the stability criterion then becomes

$$\frac{r_c}{r_o} \lesssim 0.95\left(\frac{P_o}{P_m}\right)^{1/2} M_o . \tag{25}$$

We can recast this equation into a limit on the momentum flux of the jet. First, we note that $P_o M_o^2 = 3\rho_o v_o^2/5$. We note that $P_{\rm ram} \equiv \rho v^2$ is the ram pressure in the jet and that $P_{\rm ram} r^2$ is a constant during the free expansion of the jet. Finally, we can set $r_c \approx 0.74 r_s$, $P_m \approx 1.4P_s$, and take the value of P_s from equation (3). Then, equation (25) becomes a limit on the momentum flux $P_{\rm ram} r^2$ in the jet:

$$P_{\rm ram} r^2 \gtrsim 6 \times 10^{31}\left(\frac{M_s}{1\ M_\odot\ {\rm yr}^{-1}}\right)^{1.19}\left(\frac{r_s}{\rm kpc}\right)^{-0.19}\frac{\rm g\ cm}{\rm s^2} . \tag{26}$$

In § V, we will apply these results to the radio sources associated with central dominant cluster galaxies in cooling flows.

IV. NUMERICAL EXAMPLES

a) Method of Calculation

We used the three-dimensional particles–in-cell scheme (3D–PIC) as described in Livio *et al.* (1986*a*, *b*), modified for this problem. We calculated the acceleration due to pressure forces for each cell (e.g., Harlow 1964), rather than for each particle as in the Livio *et al.* calculations. The particles in the calculations were all assigned to the jet fluid. The effect of the ambient medium was included by setting the pressure in each empty cell (a cell without any particles) to be equal to the ambient medium pressure. This code is designed to simulate steady state flow. We started by injecting particles into an empty grid; the criteria used to establish a steady state flow were similar to those used by Livio *et al.* (1986*a*). Usually a steady state was reached after two crossing times of the grid. Following the establishment of a steady state, we averaged the physical quantities over several crossing times. In one case (model 3 below), we continued the run for seven crossing times in order to check whether there was any kind of numerical instability. We found no such instability.

In order to prevent numerical instability, we found that the initial average number of particles per cell was required to be greater than six. Of course, the number of particles per cell increases after the compression of the jet. Because of the interaction between particles located in the same cell, the 3D–PIC code always has some amount of numerical viscosity and heat conductivity. However, the effective numerical viscosity decreases by a significant amount when the conservation of angular momentum is enforced in each cell during the interaction, as we have done in our implementation of the 3D–PIC. While it would be possible to reduce the numerical viscosity and heat conductivity by changing the assumed interaction parameters in the code (Livio *et al.* 1986*a*), this would also require that the spatial resolution and the number of particles be increased considerably. This increase would unfortunately require unrealistically large amounts of computer memory and computing time. It is also possible that the numerical viscosity in these calculations is not completely unphysical; it corresponds roughly to the amount of viscosity expected if turbulent viscosity is very effective.

In the rest of the paper, when we describe the numerical results we will use the initial jet radius, velocity, and density as our units of length, velocity, and density. We will generally use r to represent the distance along the jet axis in these units. In all of the calculations (other than a few tests of the code), the cell size was taken to be 0.125 in these units. We made two runs to test our numerical code. In the first, we allowed the jet to expand freely for a distance of three jet radii, and we compared the jet properties to the analytical solution for this case (eqs. [14] and [15]). The increase in the jet's radius and the decrease in its density were identical to those in the analytical solution to within the numerical errors. The Mach number was 5%–10% smaller than in the analytic solution, and the pressure was greater by 15%. We attribute these differences to the finite resolution and to the numerical viscosity and heat conductivity in our code.

In a second test, we modeled the flow in an underexpanded jet where the fluid was air ($\gamma = 1.4$). The cells size in this run was 0.25; that is, the initial jet radius was resolved into only four cells. The jet expanded to a radius of 10 cells. The initial Mach number of the jet was taken to be 2, and the ratio between the initial thermal pressure in the jet and the ambient medium pressure was taken to be 3.5. We did not find any obvious Mach disk in this model. According to Chang and Chow (1974), this model should produce a Mach disk with a radius equal to half the initial jet radius. Unfortunately, with our resolution it is very difficult to really tell whether or not the flow has such a small Mach disk. In addition, Ladenburg, Van Voorhis, and Winckler (1949) failed to find a Mach disk in experiments on underpressured jets having a pressure ratio of 3 and an initial Mach number of unity.

As a second check on our solutions for an underexpanded jet in air, we determined the position of the first shock in the flow in our underexpanded jet model. For our assumed flow parameters, the distance from the initial position of the jet to the first shock (measured along the symmetry axis of the jet) should be $r = 6.5$ units, based on experiments by Adamson and Nicholls (1959) and Chang and Chow (1974). The experiments show that the lowest density region is just in front of the first shock, where the maximum density gradient occurs (Ladenburg, Van Voorhis, and Winckler 1949). Probably because of the smearing produced by the numerical viscosity in our code, the minimum density region in our model was found to be at a distance of 7.5 units, while the maximum density jump occurred at 9.5 units. If we take the position of the shock to be the mean of these two values, the distance to the first shock is 8.5 units, which is somewhat higher than the experimental value. We can suggest at least four possible reasons why our numerical calculations give a larger distance to the first shock. First, this may be due to the numerical viscosity and heat conductivity in our code, which tend to smear out the abrupt shock transition (see also Williams and Gull 1984). Second, the low spatial resolution of the calculations might have a similar effect. Third, in our models no fluid particles were used to model the ambient gas. For numerical reasons, the ambient pressure was assumed only to apply in completely empty cells (there is no "partial pressure" of the ambient gas in nonempty cells). This may have effectively lowered the ambient pressure in our models somewhat below that which we assumed. Finally, there may be a boundary layer between the jet and the ambient medium in the experiments. Such a boundary layer would transfer momentum from the jet to the ambient medium and reduce the resulting Mach number of the jet (Lau 1981; Williams and Gull 1984). Since no particles are used to model the ambient medium in our code, there can be no such boundary layer in our models.

As another test of the underexpanded jet model, we also compared the qualitative features in plots of the gas density in our model with the experimental results of Ladenburg *et al.* (1949); only qualitative comparisons were possible because all extent experiments have been done with Mach numbers or pressure ratios (or both) which are different from those we used in our model. We found that the density plots showed a good qualitative agreement.

In order to test the possible influence of our finite spatial resolution, we also repeated two of our calculations (models 8 and 10 below) with the cell size doubled (0.25 units). Then, the initial jet radius was spanned by only four cells. The qualitative features in the flow were unchanged, and no flow variable was altered by more than 20%.

Because of the obvious problems discussed above, and also considering the fact that our code was written for steady state flow and cannot treat instabilities, we will regard our numerical results as more qualitative than quantitative. We will only use the numerical models to discuss the gross structure of jets and will not attempt to apply the models in any detail.

TABLE 1

STRAIGHT JET MODELS

Model	M_1	$\frac{P_{amb}}{P_{ram}}$	$\frac{P_{amb}}{P_1}$	$\frac{\rho_{max}}{\rho_1}$	$\frac{\Delta}{R_j}$	$\frac{P_{max}}{P_{amb}}$	$\frac{P_{steady}}{P_{amb}}$	$\frac{R_{Mach}}{R_j}$	M_{min}	$\frac{W}{R_j}$
1[a]	8	0.08	8.4	4.0	4.9	1.4	0.60	0.25	4.0	...
2[a]	8	0.31	33.5	7.0	2.0	2.6	0.78	0.25	1.5	4
3[a]	20	0.31	210	8.5	2.1	2.6	0.73	0.25	1.6	4
4[b]	8	0.31	33.5	8.2	3.6	2.0	0.74	0.35	2.1	4
5[b]	8	0.94	101	8.7	2.3	2.4	0.87	0.25	0.8	...

[a] Models 1–3 have "step function" ambient pressure profiles in which the ambient pressure rises instantaneously from zero to the value in this table at $r = 0.625$—see eq. (27).

[b] Models 4 and 5 have a linear pressure gradient up to the full ambient pressure given in this table—see eq. (28).

b) Numerical Results

i) *Straight jets*

Although our main goal is the simulation of bent jets, we have done several calculations with a cylindrical symmetry. These were done in order to check the assumptions made in our analytic calculations of the previous section, and in order to produce a basis set of straight jet models compared to the bent jets. Because the pressure gradients at sonic radii in cooling flows are quite narrow, these calculations have been done in plane-parallel rather than spherical geometry. For consistency, we will continue to use r to represent the distance along the direction of propagation of the jet.

A total of five straight-jet models were run; the parameters assumed for the jets are given in Table 1. As before, R_j, P_1, ρ_1, v_1, and M_1 are the initial jet radius, pressure, density, velocity, and Mach number, respectively; P_{ram} is the initial ram pressure in the jet; $P_{ram} = \rho_1 v_1^2$; and P_{amb} is the maximum ambient gas pressure assumed in the models. In models 1, 2, and 3, the jet encounters a discrete jump in the ambient pressure (from zero to the value given in Table 1) at the fifth cell or at $r = 0.625R_j$, so that

$$P(r) = P_{amb} \times \begin{Bmatrix} 0 & r < 0.625R_j \\ 1 & r \geq 0.625R_j \end{Bmatrix} \tag{27}$$

In models 4 and 5, the discrete jump is replaced by a linear pressure increase up to P_{amb}:

$$P(r) = P_{amb} + \begin{Bmatrix} 0 & r < 0.625R_j \\ \left(\frac{r - 0.625R_j}{3R_j}\right) & 0.625R_j \leq r < 3.625R_j \\ 1 & 3.625R_j \leq r \end{Bmatrix} \tag{28}$$

In all of these models, we took $\gamma = 5/3$.

The results of our calculations for straight jets are summarized in Table 1 and Figures 3 and 4. In Table 1, ρ_{max} is the maximum density in the jet, which always occurs just behind the first shock in the jet, and Δ is the distance from the point at which the ambient medium pressure first occurs ($r = 0.625R_j$) to the point in the jet at which the maximum density occurs. We use P_{max} to denote the maximum value of the pressure in the jet, which occurs just after the first shock in the same region where ρ_{max} is found; M_{min} is the smallest Mach number in the jet, and this also occurs just after the first shock. In all of these cases, the first shock contains a Mach disk (a transverse shock); R_{Mach} is the radius of this Mach disk. The values for R_{Mach} are rather crude estimates since the Mach disk is not highly resolved in our calculations. In models 2–4, a second shock (or more explicitly, a second density maximum) is found further down the jet. The distance between the first and second density maxima is given by W. Finally, P_{steady} is the pressure in the jet at large r after the jet has reached a steady pressure and a constant radius. This steady pressure is less than the ambient pressure because in our code the effective numerical ambient pressure is $\sim 80\%$ of the pressure we put into each cell.

In Figures 3 and 4 we present the density in the midplane of the jet (the plane through the symmetry axis) for models 2 and 4, respectively. The area of the square drawn at each cell is proportional to the density in that cell. The small asymmetries in the model densities near the edges of the jets is due to fluctuations in the number of particles in these cells which are averaged over only a finite time. We only show the density in cells for which the average number of particles is greater than one.

The slope of the linear pressure gradient in models 4 and 5 was chosen so that $\beta \approx 10^{-1}$ in equation (23). In models 1–3 the pressure is discontinuous; these cases are useful in assessing qualitative effects of a very steep pressure gradient. We see that the maximum pressure in the jet, which occur on the symmetry axis immediately after the shock, is typically larger by a factor of two than the external pressure. This suggests that the assumption made in the previous section (that the postshock pressure was the same as the ambient pressure) was somewhat low, but not terribly far off. The pressure decreases to ~ 1.5 times the external pressure as one moves from the symmetry axis to the edge of the jet. After the shock region, the pressure in the jet falls to a value which is less than ($\sim 70\%$) the ambient medium pressure (however, see the comment about the effective numerical ambient pressure above).

In Figure 5, we display the points along each streamline of the flow where the largest density gradient (largest density jump between adjoining cells) occurs. A few interesting features appear immediately from these plots. First, we see that the geometry of the

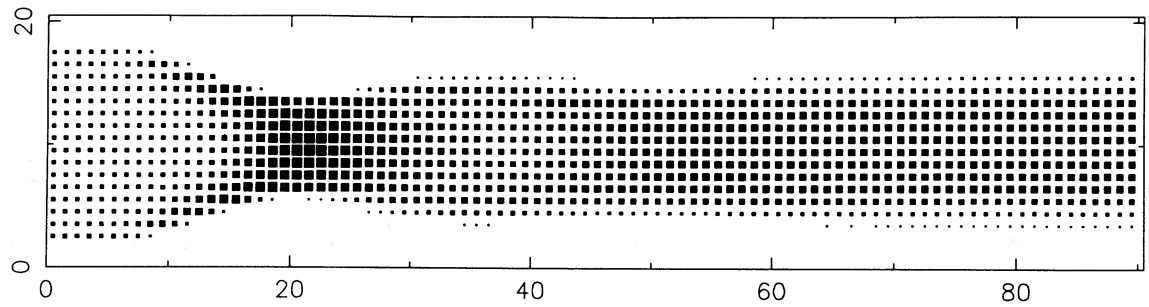

FIG. 3.—Density in the mid-plane of the jet (the plane through the symmetry axis) for model 2. Area of the square drawn at each cell is proportional to the density in that cell. Density is not shown for cells for which the average number of particles is less than one. The abscissa is the distance along the direction of propagation of the jet; the ambient medium starts at 5 units. The ordinate measures distance across the jet; the jet is centered at 10 units and has an initial radius of 8 units.

shocks for the models with different Mach numbers (8 and 20) but the same $P_{\rm ram}$ are similar, as predicted by equation (23). Second, there is clearly a Mach disk at the first shock, although with our resolution it is difficult to accurately determine its size. Third, the shock in model 4 does not appear to start immediately after the region where the jet pressure equals the ambient pressure (see also Fig. 3).

Thus, the assumptions made in the previous section concerning the geometry of the shock (conical) and the starting point of the shock are not completely accurate.

In the models with a high ambient pressure (models 2–5), the Mach number behind the shock is low. Thus, we expect these jets to be fairly unstable. At a lower ambient pressure (model 1), and to some extent for the more gradual pressure gradient (model 4), the shock tends to be weaker, as one might expect. Somewhat surprisingly, the maximum density in model 4 is higher than in model 2, although these models have the same maximum ambient pressure and model 4 has the smaller pressure gradient.

The "wavelength" W separating shocks in models 2–4 is $W \approx 4R_j$, which is ~ 2.5–3 times the diameter of the jet at that part of the flow. This is in basic agreement with the results of Norman, Smarr, and Winkler (1985). In models 1 and 5, we didn't find a second shock, although it is possible that this is due to the numerical viscosity in our calculations.

Burns, Norman, and Clarke (1986) have calculated the structure of a jet running into a region of *decreasing* external pressure. In their models, Mach disks occurred only when the scale height of the external pressure was smaller than the jet radius. They also found that the Mach number behind the Mach disk was always less than unity. They argued that the same phenomenon should exist in the increasing external pressure. Our calculations would appear to partially confirm this conjecture.

The linear ambient pressure profiles in models 4 and 5 allow us to test our analytic calculations for the stability of jets (eq. [25]). We can take $r = r_o$, $P_o = P_1$, and $M_o = M_1$. Then, the right-hand side of equation (25) is 1.3 for model 4 and 0.75 for model 5. Thus, we would expect the minimum Mach number in model 4 to be slightly supersonic, while model 5 would become subsonic. We see that for model 4 the minimum Mach number is 2.1, which is slightly supersonic. In model 5, the minimum Mach number is 0.8, which is subsonic.

We would like to emphasize again that although our condition for instability in the previous section was that the jet become subsonic, even if $1 < M_{\rm min} \lesssim 2$, the jet may still be unstable. We should also point out that, in the region beyond the first strong shock, Kelvin-Helmholtz and Rayleigh-Taylor instabilities may also disturb the jet. In this region, the density contrast of the jet ($\rho_j/\rho_{\rm amb}$) can affect the stability of the jet, in addition to the pressure contrast ($P_j/P_{\rm amb}$) and the Mach number (Norman, Smarr, and Winkler 1985).

ii) *Bent Jets*

For a cooling flow onto an elliptical galaxy, the sonic surface (on which the inflow velocity equals the sound speed) will generally be ellipsoidal in shape. In addition, if the cooling gas has any angular momentum, this may also cause the sonic surface to be nonspherical. Unless a radio jet propagating along one of the principal axes of the sonic surface, it will typically encounter the sonic surface of the cooling flow at an oblique angle. This may result in a deflection of the jet, in addition to the possibility of the jet becoming unstable. To study this situation, we performed six simulations of the flow which occurs when a jet enters a region of high

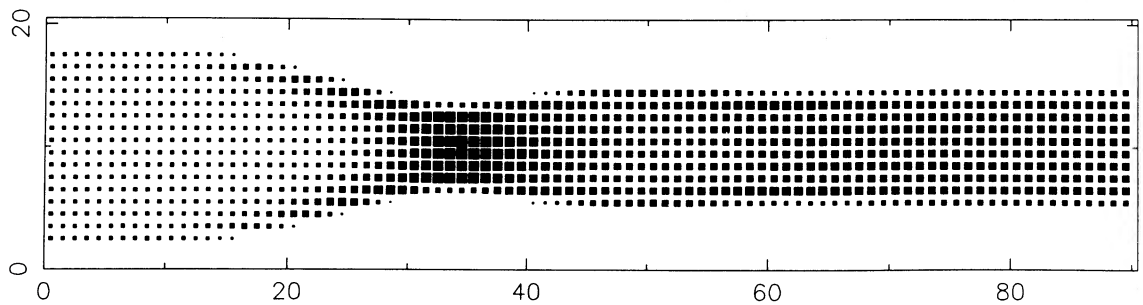

FIG. 4.—Density in the midplane of the jet for model 4, in same format as Fig. 3

TABLE 2

BENT JET MODELS

Model	γ	M_1	$\frac{P_{amb}}{P_{ram}}$	$\frac{P_{amb}}{P_1}$	α	$\Delta\alpha$	$\Delta\alpha_{est}$	$\frac{\rho_{max}}{\rho_1}$	$\frac{P_{max}}{P_{amb}}$	M_{min}
6[a]	5/3	8	0.314	33.5	25	6	8	6.1	2.4	1.4
7[a]	5/3	8	0.314	33.5	45	20	17	4.2	1.4	1.8
8[a]	5/3	20	0.157	105.0	45	7	9	5.3	2.0	2.7
9[a]	5/3	20	0.314	210.0	45	20	17	4.7	1.4	1.8
10[b]	5/3	20	0.314	210.0	45	10	...	6.8	1.3	2.6
11[a]	4/3	20	0.314	168.0	45	17	17	10.1	1.8	2.7

[a] Models 6–9 and 11 have "step function" ambient pressure profiles in which the ambient pressure rises instantaneously from zero to the value in the table at $x = 0.625$—see eq. (27) with $r \to x$.

[b] Model 10 has a linear pressure gradient up to the full ambient pressure given in the table—see eq. (28) with $r \to x$.

ambient pressure at an oblique angle to the direction of the pressure gradient. Again, because the jets themselves and the regions of pressure increase at the sonic radii of cooling flows are both quite narrow, we have adopted plane-parallel rather than ellipsoidal geometry. We assume that the ambient medium pressure is a function of only one coordinate, taken to be x. The ambient medium pressure is zero for $x < 0.625R_j$. Thus, the sonic surface is effectively parallel to the y-z plane. The jet propagates in the x-y plane and is initially moving in the $+x$ and $+y$ direction at an angle of α to the x-axis. Thus, α is the angle between the direction of the initial jet velocity and the direction of the gradient in the ambient medium pressure (i.e., the normal to the ambient medium boundary).

The results of these calculations are summarized in Table 2 and in Figures 6–9. The notation is similar to that in Table 1. $\Delta\alpha$ is the angle of deflection of the jet, which was determined from the line-of-propagation of the geometric center of the jet near the downstream end of the numerical grid. Of course, the sense of the deflection is to increase α. Because the edges of the postshock jet are usually not exactly parallel (i.e., the jet is oscillating) and the density is inhomogeneous, the values of $\Delta\alpha$ are only accurate to about 10%. From Table 2, we see that the angle of deflection of the jet $\Delta\alpha$ increases with increasing ambient medium pressure and with increasing jet incident angle α.

From Tables 1 and 2, we see that the shock gets weaker and M_{min} increases as α increases; for example, compare model 2 to models 6 and 7, or model 3 to model 8. This suggests that the jet is actually more stable if it encounters the sonic surface obliquely (all other things being equal).

A crude estimate of $\Delta\alpha$ can be obtained in the following manner. Let us refer to the side of the jet closest to the x-axis as the "underside" and the side closest to the y-axis as the "topside." Of course, the underside of the jet encounters the region of high ambient pressure before the topside does. Nonetheless, we will neglect the fact that the underside of the jet will start to bend before the topside. We will neglect the compression of the jet in the z-direction when it enters the region of high ambient pressure; we will assume that the thickness of the jet in the z-direction remains constant at $2R_j$. None of these assumptions are really justifiable and they are not supported by the numerical calculations. Referring to Figures 6–9, we see that under these assumptions the underside of the jet passes a distance of $2R_j \tan\alpha$ into the high-pressure ambient medium before the topside has fully entered this region. Integrating the pressure force on this section of the jet, we find that there is a force whose direction is perpendicular to the initial direction of motion of the jet. In a time Δt, this force imparts a momentum $\Delta p = P_{amb}\pi R_j^2 \Delta t \tan\alpha$. The momentum passing

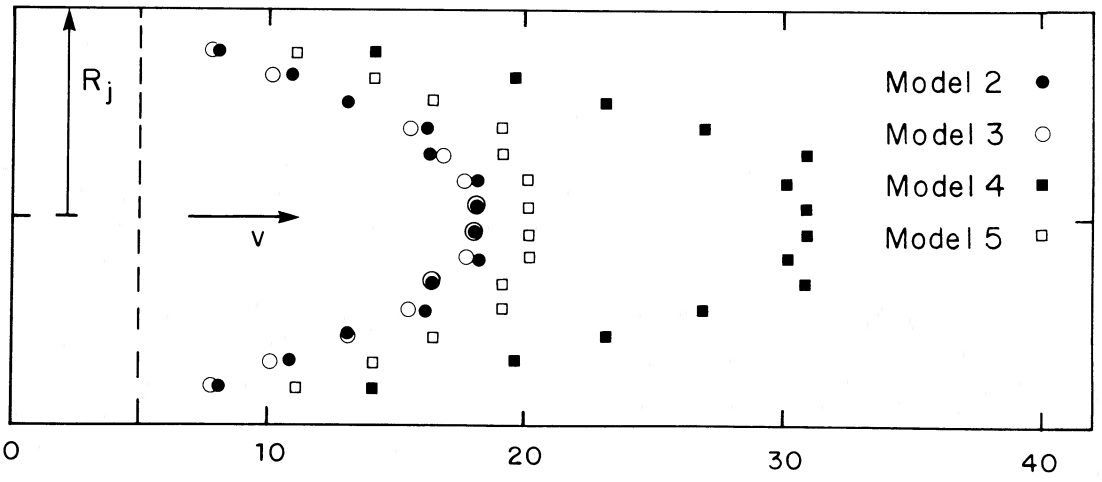

FIG. 5.—For several models, this figure shows the points along each streamline of the flow at which the largest density gradient (largest density jump between adjoining cells) occurs. Dashed line indicates the position at which the ambient medium starts.

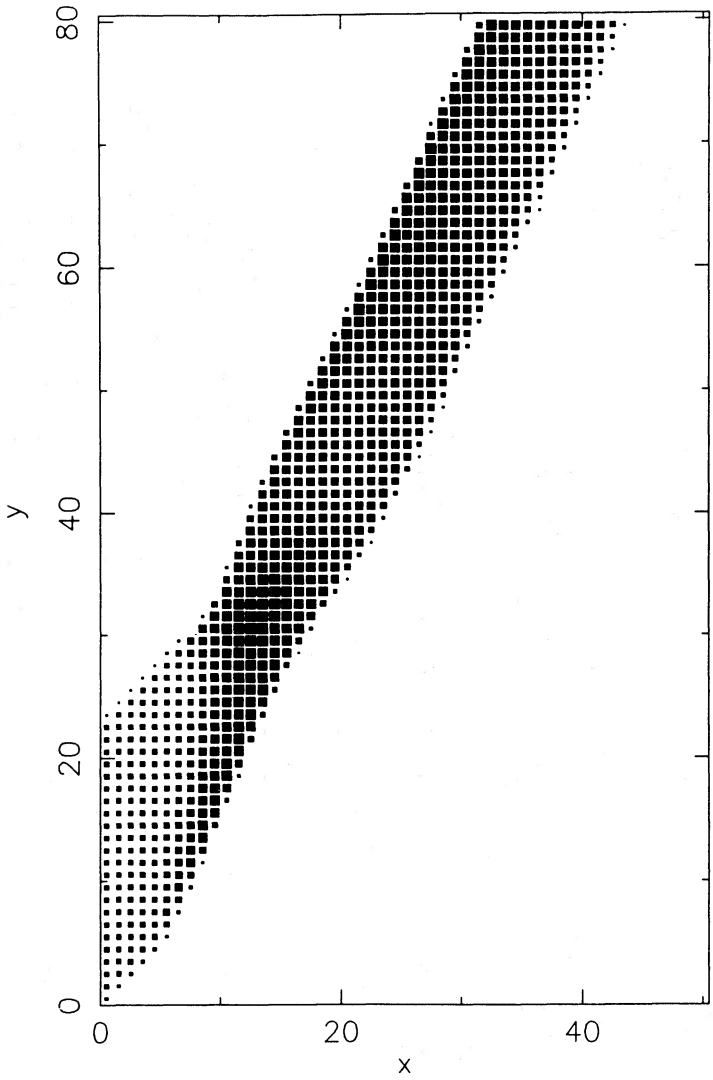

FIG. 6.—Density in the symmetry plane of the jet for model 9. Format is similar to that in Fig. 3. The density of the ambient medium is a function of x only, and starts at $x = 5$ units. The jet propagates at an angle $\alpha = 45°$ to the x-axis, and the x-y plane is the plane of reflection symmetry. The jet has an initial radius of 8 units.

through the cross section of the jet in that same time is $p = \pi R_j^2 \rho_1 v_1^2 \Delta t$, so that the deflection angle is given approximately as $\Delta\alpha \approx \Delta\alpha_{\rm est}$, where

$$\tan \Delta\alpha_{\rm est} = \frac{\Delta p}{p} = \frac{P_{\rm amb}}{P_{\rm ram}} \tan \alpha \, . \tag{29}$$

We give values of $\Delta\alpha_{\rm est}$ from equation (29) in Table 2. As can be seen, this crude estimate gives surprisingly accurate estimates of the deflection angle. For model 10, the simple treatment given above not apply, because of the gradual pressure rise assumed in that case.

In Figure 6, we present the jet density in model 9. The density is shown in the symmetry plane of the jet, $z = 0$, and the density is proportional to the area of the black square drawn at each cell in the numerical grid. Figure 7 gives the integrated (projected) density perpendicular to the symmetry plane

$$N \equiv \int \rho \, dz \tag{30}$$

for the same model. In Figure 8, we show a map of the jet velocity field, again in the symmetry plane of the jet $z = 0$. Because the velocity field is relatively uninteresting before the shock or well after it (nearly parallel, constant velocities), we show only the region near the shock where the jet first enters the ambient medium. For purposes of comparison, Figure 9 shows the density in the symmetry plane for model 10, which has a more gradual increase in the pressure.

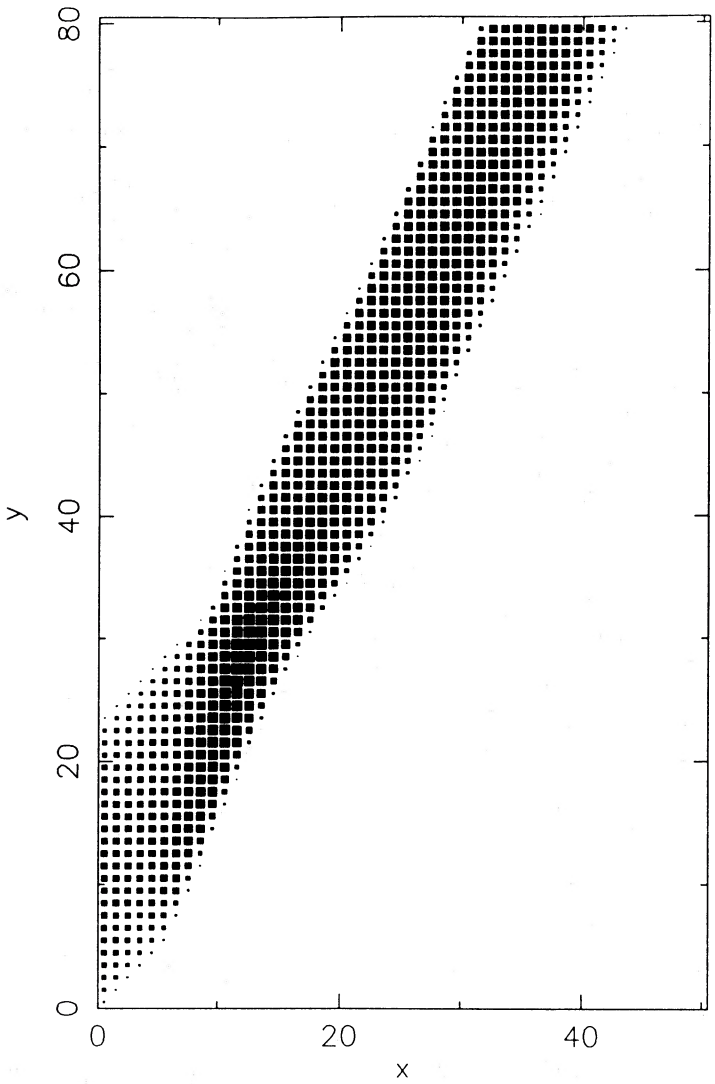

FIG. 7.—Projected density N (see eq. [30]) of the jet in model 9. The format is similar to that in Fig. 6. The area of the square drawn at each cell is proportional to the projected density at that position. For purposes of normalization, we note that the central projected density of the initial jet is $N_1 = 2\rho_1 R_j$, and that the maximum value of N in the figure is $\sim 3N_1$.

From Figures 6 and 9 (and from similar figures for the other models which we haven't presented here), one can see that the density in the topside of the jet is higher than in the underside. This asymmetry may lead to a kink instability in the jet (Norman, Smarr, and Winkler 1985).

V. DISCUSSION

First, we address the question of whether any of the dominant features of the morphology of radio emission from elliptical galaxies can be explained by the interaction between radio jets and the steep pressure gradients inside the sonic radii of cooling flows.

For "normal" elliptical galaxies (taken here to mean those not located at the centers of rich clusters of galaxies, and excluding narrow-angle-tail sources), the dominant radio morphologies are those of large doubles and straight jets, with the average size being on the order of 300 kpc (see, for example, the review by Miley 1980). As discussed in § II, these galaxies generally seem to have cooling flows powered by stellar mass loss from within the galaxy, with $\dot{M} \lesssim 1\ M_\odot\ \mathrm{yr}^{-1}$. The sonic radii for these cooling flows are expected to be $\lesssim 100$ pc (see eq. [1] and Sarazin and White 1987). Thus, disruption of radio jets at the sonic radii of these cooling flows must not be occurring.

At first, it would seem that the wide-angle tail (WAT) sources associated with central dominant cluster galaxies would be more promising candidates for jet disruption at cooling flow sonic radii. First, many clusters of galaxies have very large cooling flows with typical inflow rates of $\dot{M} \approx 100\ M_\odot\ \mathrm{yr}^{-1}$. Larger inflow rates produce larger sonic radii (eq. [1]). Second, WATs are typically somewhat smaller than the double radio sources associated with normal elliptical galaxies. Recently, O'Dea and Baum (1987) observed a number of radio sources associated with central dominant cluster galaxies in clusters with cooling flows, and compiled

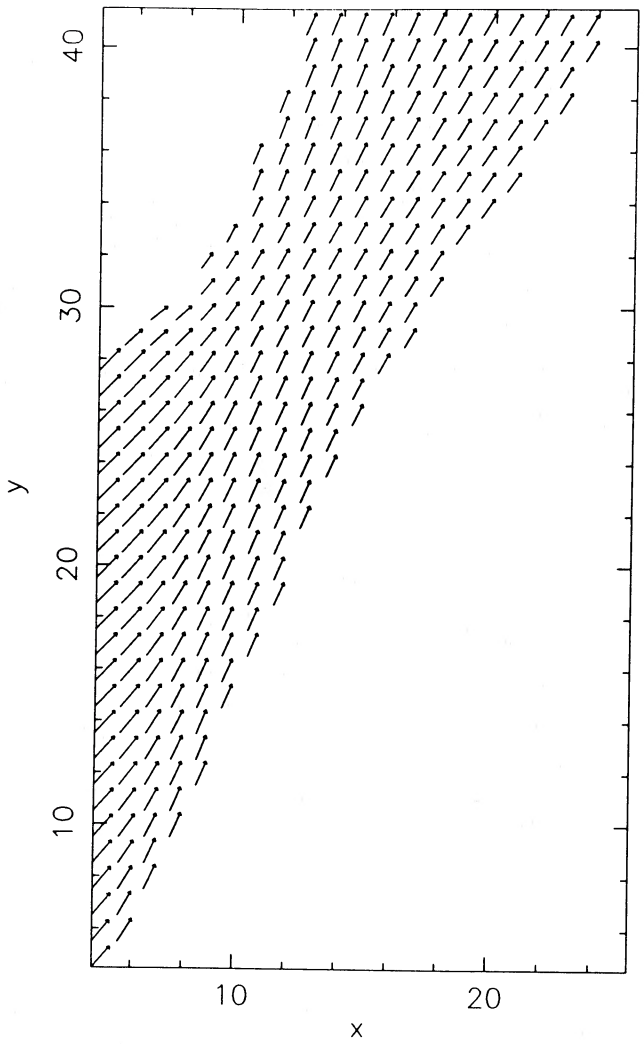

FIG. 8.—Jet velocity field in the symmetry plane of the jet for model 9. Only the region of the model near the shock is shown; further upstream or downstream the velocity field is uniform. The length of each arrow is proportional to the jet fluid velocity, and the direction shows the direction of the flow.

their measurements with previous results. Figure 10 shows the largest linear size (LLS) of these radio sources, plotted against the cooling rate $\dot{M}$ in the associated cluster. It appears that large radio sources are only associated with clusters with small inflow rates, suggesting some connection between the origin of WAT radio galaxies and cooling flows. However, all of the radio sources with measured structure are still quite large; the average measured value of LLS is 50 kpc. This is much larger than the expected value of the sonic radius, even for the large cooling rates in these clusters (eq. [1]). Even noting that the LLS (which is the largest *diameter* of the radio source) is likely to be several times the *radius* at which the jet is first disrupted, it seems unlikely that the morphology of WAT radio sources is due to jet disruption at the cooling flow sonic radius in most cases.

It is possible that the sonic radii of cooling flows have been greatly underestimated? Considering equation (1), it would seem that this would be possible if the temperatures at the sonic radii are very low, $T_s \lesssim 10^5$ K. Unfortunately, such a low temperature at the sonic radii is inconsistent with solutions which match on to outer atmospheres in hydrostatic equilibrium with galactic or cluster potentials (White and Sarazin 1987*c*; Sarazin and White 1987). In addition, if cooling flows in clusters or in normal elliptical galaxies had sonic radii as large as those required to explain the structure of the radio sources, then relatively nearby examples would show "holes" in their X-ray surface brightness profiles. No such holes are seen. Finally, we note that most of the effects which are often neglected in the theoretical treatment of cooling flows (such as thermal conduction, mass loss from the flow due to thermal instabilities, or the pressure due to magnetic fields) would tend to *decrease* the sonic radius even further. Thermal conduction keeps the gas hotter in to smaller radii and lowers the inflow velocity by replacing a portion of the enthalpy flux with conducted heat flux. Thermal instabilities lower the density of the ambient gas (reducing its cooling rate so that it stays hotter) and also lower the mass flux and thus the inflow velocity. Magnetic fields make the gas less compressible (Soker and Sarazin 1987).

However, Sumi *et al.* (1988) note that some radio sources associated with cD galaxies *do* show interesting radio structures on small scales which may very well be due to interactions between the radio jets and a pressure wall at the sonic radio of a cooling flow. The radio jets associated with the cD galaxies in the clusters A1795 and A2029 both have two knots of strong radio emission at roughly symmetrical positions away from the nucleus (van Breugel, Heckman, and Miley 1984; Sumi *et al.* 1988). The radio sources

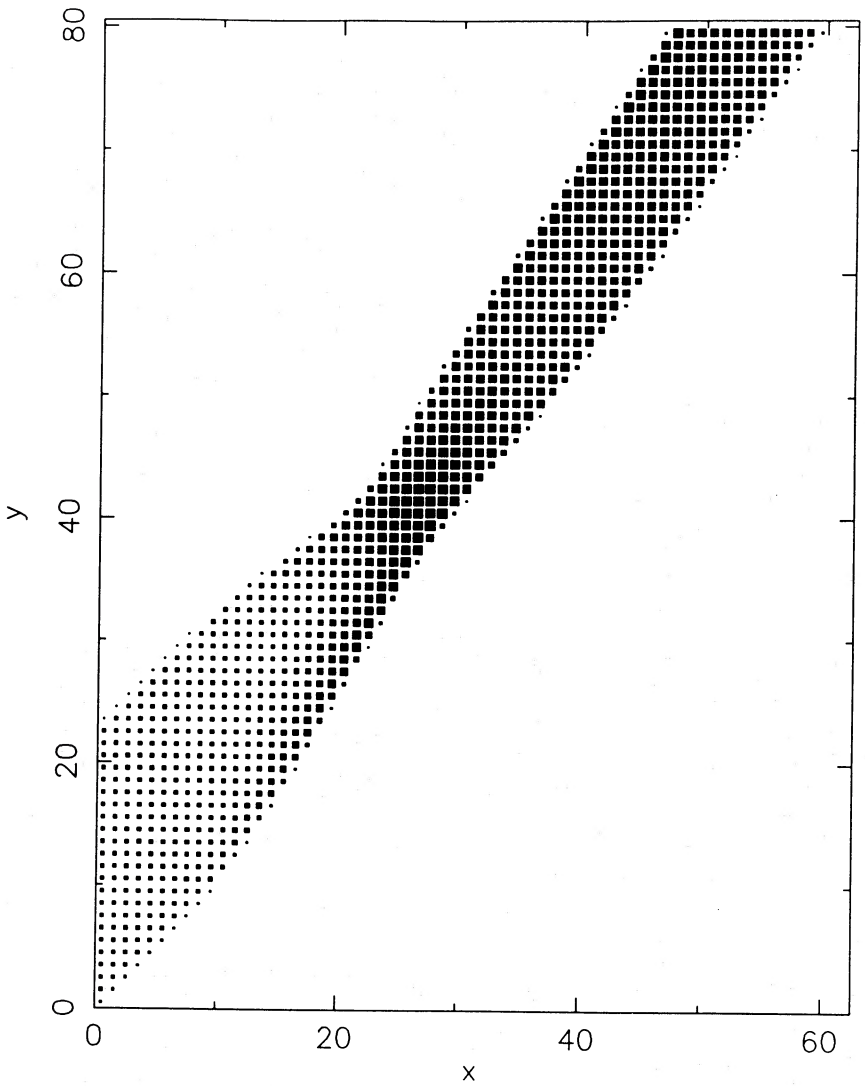

FIG. 9.—The projected density N (see eq. [30]) of the jet in model 10. The format is similar to that in Fig. 7.

in M87 and NGC 1275 show similar knots on one side of the nucleus (Owen, Hardee, and Bignell 1980; Pedlar, Booker, and Davies 1983; Sumi *et al.* 1988). All of these galaxies are at the centers of cooling flows.

In IC 1101, the cD galaxy in A2029, the knots are located at average projected radii of ~ 2.6 kpc (Sumi *et al.* 1988). Beyond the knots, the radio jets broaden and wiggle, and Sumi *et al.* suggest that they have become subsonic. Let us assume that the knots correspond to the radius of the pressure wall r_c, so that the sonic radius is $r_s \approx 3.5$ kpc. The global inflow rate in this cluster is $\sim 320\ M_\odot\ \mathrm{yr}^{-1}$ at the cooling radius of 200 kpc (Arnaud and Fabian 1987). Detailed deconvolutions of the X-ray surface brightness profiles in many clusters suggest that the inflow rate varies crudely as $\dot{M} \propto r$ (Thomas, Fabian, and Nulsen 1987), which implies that $\dot{M}_s \sim 6\ M_\odot\ \mathrm{yr}^{-1}$. Then, equation (1) would require $T_s \approx 9 \times 10^5$ K (Sumi *et al.* 1988). Unfortunately, it is clear from White and Sarazin (1987*c*) that this temperature is much too low (by one order of magnitude) to match onto any cooling flow solution which is consistent with the X-ray properties of the cluster at large radii. On the other hand, perhaps the variation of $\dot{M}$ with radius inferred from the X-ray surface brightness profiles is greatly in error, and $\dot{M}_s \approx 10^2\ M_\odot\ \mathrm{yr}^{-1}$. In this case, the required sonic radius temperature is $T_s \approx 3 \times 10^6$ K, which is still rather low but perhaps not impossibly so.

In 4C 26.42, the radio source associated with the cD galaxy in A1795, there are two knots with an average separation from the nucleus of 1.5 kpc (van Bruegel *et al.* 1984; Sumi *et al.* 1988). The distances of the two knots from the nucleus differ by roughly a factor of 2. The global inflow rate in this cluster is $\sim 340\ M_\odot\ \mathrm{yr}^{-1}$ at the cooling radius of 240 kpc (Arnaud and Fabian 1987). The same arguments given above for A2029 would require a sonic temperature of 8×10^5 K if $\dot{M} \propto r$ or $\sim 3 \times 10^6$ K if $\dot{M}_s \sim 10^2\ M_\odot\ \mathrm{yr}^{-1}$; again, these values are rather low. The jets in 4C 26.42 bend very sharply and symmetrically just beyond the knots, giving the source an overall S-shaped structure. The jets also broaden as they bend. If the knots are due to the interaction of jets with the pressure wall near the sonic radius of the cooling flow, it is possible that the jets encounter the pressure wall at an oblique angle. In § IV*b*(ii), we showed that this can lead to a sharp bending of radio jets.

In both A2029 and A1795, the knots in the radio jets occur on very small scales compared to LLS, the largest linear size of the

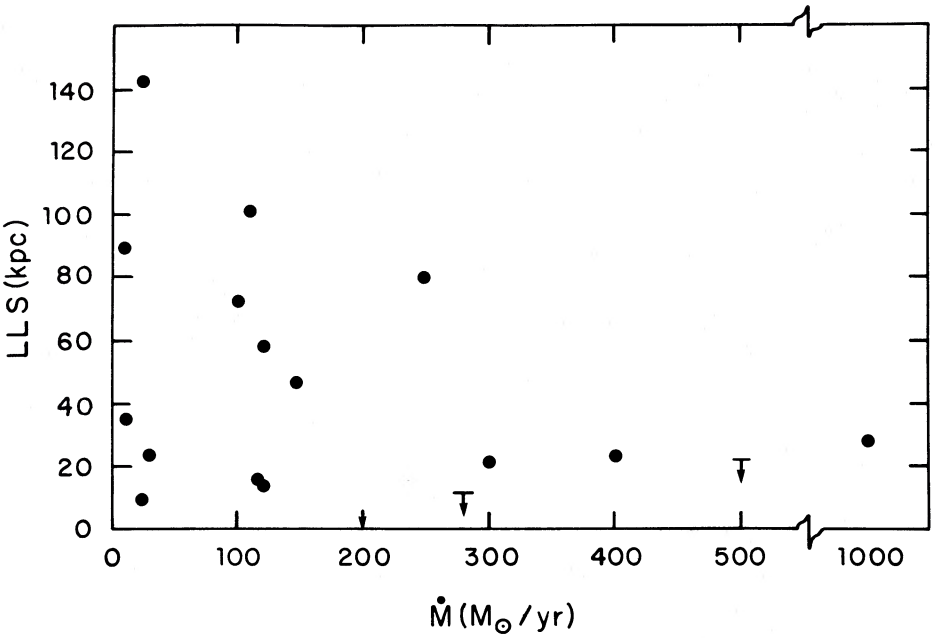

FIG. 10.—The largest linear size (LLS, in kpc) for radio sources associated with the central dominant galaxies in cooling flow clusters plotted vs. the cooling rates for these clusters $\dot{M}$ (in $M_\odot$ yr^{-1}), from O'Dea and Baum (1987). Note the break in the abscissa between 500 and 1000 $M_\odot$ yr^{-1}.

radio structure. The values of LLS are 23 kpc in A1795 and 80 kpc in A2029 (O'Dea and Baum 1987). If the jets are indeed decelerated to subsonic speeds at the observed knots (whatever the mechanism), they must somehow manage to continue to propagate to much larger distances. Sumi *et al.* (1988) have suggested that the large-scale "jets" in many WAT radio sources, other sources associated with galaxies at the centers of cluster cooling flows, and perhaps many other FR class I radio sources are possibly just subsonic, buoyant plumes and not well-collimated supersonic jets (see also Bicknell 1986). If this were indeed the case, our objections to the disruption of radio jets at the cooling flow sonic radii would disappear, and this mechanism could play a major role in determining the structure of radio sources.

We conclude that jet disruption at the cooling flow sonic radius is probably not the primary cause of the morphology of radio sources associated either with normal elliptical galaxies or with central dominant cluster galaxies. The fact that these radio sources generally show much larger structures indicates that radio jets survive disruption at these sonic radii, although it is also possible that the larger scale "jets" are really just subsonic, buoyant plumes. In several cluster central radio sources, the jets do indeed show knots, broaden, and undergo sharp bends or wiggles on scales which could be attributed to cooling flow sonic radii.

If radio jets are *not* disrupted at cooling flow sonic radii, we can suggest two possible explanations. First, it may be that such sonic radii don't exist (that is, cooling flows may remain fully subsonic) or that the pressures at the cooling radii are much smaller than indicated by simple models. The latter would be most likely to occur if the mass flux at the sonic radius is much smaller than the mass flux at larger radii inferred from X-ray observations. Unfortunately, the extant X-ray observations have insufficient spatial resolution to directly measure the gas properties at the expected sonic radii. Second, it may be that the jets in these radio sources are sufficiently robust that they are not disrupted at the sonic radius. Again, it is unfortunate that typical radio observations do not resolve the jet on the scale at which sonic radii are expected.

According to equation (26), the stability of jet propagation through a cooling flow sonic radius depends on the momentum flux in the jet. Assuming that the Mach number of the jet is large, the total energy flux in the jet is $L_j = \rho_j v_j^3 \pi R_j^2/2 = \pi P_{\rm ram} r^2 v_j \beta^2/2$, where ρ_j and v_j are the jet density and velocity, respectfully, and we recall that $\beta \equiv R_j/r$. Let $\eta \equiv L_r/L_j$ be the efficiency of conversion of the energy in the jet into the extended radio luminosity L_r. Then, the condition that the jet not be disrupted becomes (eq. [26])

$$\left(\frac{L_r}{10^{40}\ \mathrm{ergs\ s^{-1}}}\right) \gtrsim 0.3 \left(\frac{v_j}{c}\right)\left(\frac{\eta}{0.1}\right)\left(\frac{\beta}{0.1}\right)^2 \left(\frac{\dot{M}_s}{1\ M_\odot\ \mathrm{yr}^{-1}}\right)^{1.19} \left(\frac{r_s}{\mathrm{kpc}}\right)^{-0.19} . \tag{31}$$

For the jet in 3C 120 (which is nearly unique in having radio observations of the distance scale where the sonic radius is expected), the observations do indeed give $\beta \approx 0.1$ (Walker, Benson, and Unwin 1987). For purposes of comparison to the radio observations, it is useful to estimate $L_r \approx \nu P_\nu$, where P_ν is the radio power observed at a frequency ν. Thus, $L_r = 10^{40}$ ergs s^{-1} corresponds to $P_{1400} \approx 10^{24}$ W Hz^{-1} at $\nu = 1400$ MHz and to $P_{178} \approx 10^{25}$ W Hz^{-1} at $\nu = 178$ MHz.

In the O'Dea and Baum (1987) survey of radio sources associated with central dominant galaxies in cooling flow clusters, the medium radio power was $P_{1400} \approx 3 \times 10^{24}$ W Hz^{-1}. We assume $L_r \approx P_{1400} \times 1400$ MHz. The typical cooling rate is $\dot{M} \approx 100\ M_\odot$ yr^{-1}. Thus, one would have expected these sources to have been disrupted, unless $v_j \lesssim 0.06c$ or $\dot{M}_s \lesssim 9\ M_\odot$ yr^{-1}.

For normal elliptical galaxies, the radio luminosity function has a break at about $P_{178} \approx 4 \times 10^{25}$ W Hz^{-1} (Auriemma *et al.* 1977). Perhaps connected with this is the fact that radio sources of high radio power ($P_{178} \gtrsim 2 \times 10^{26}$ W Hz^{-1}, Fanaroff and Riley Class II) are almost all edge-brightened doubles, while lower luminosity radio sources (Class I) are more relaxed in their morphol-

ogy (Fanaroff and Riley 1974). However, even the Class I sources are typically much larger (~ 200 kpc) than the expected sonic radii in these sources. Assuming $\dot{M} \approx 1\ M_\odot\ \mathrm{yr}^{-1}$ and $r_s \approx 100$ pc in these galaxies implies that a source with $P_{178} \ll 4 \times 10^{24}$ W Hz^{-1} should be disrupted according to equation (31), unless $v_j \ll c$ or unless very little of the gas seen in the X-ray observations at large radii to be cooling actually flows into the sonic radius (that is, $\dot{M}_s \ll \dot{M}$).

We conclude that for radio sources associated with central dominant cluster galaxies and for low-luminosity elliptical galaxy radio sources in general, either the radio jets are slow and heavy ($v_j \ll c$) at distances of 0.1–1 kpc from the galaxy center, or the jets at larger scales are really subsonic, buoyant plumes, or very little of the material seen to be cooling in X-ray observations at larger distances from the centers of these galaxies ever passes through a sonic radius near the galactic center. There are several reasons why the latter might occur. For example, thermal instabilities might remove most of the gas from the inflow before the sonic radius is reached, or thermal conduction might provide enough of the energy flux so as to significantly reduce the inflow rates in cooling flows, or the pressure associated with magnetic fields might prevent inflow on the small scales associated with the sonic radii in cooling flows.

We thank Jack Burns and Dean Sumi for very helpful discussions. This work was supported in part by NASA Astrophysical Theory Center grant NAGW-764, and National Science Foundation grant AST-81-20260.

REFERENCES

Adamson, T. C., and Nicholls, J. A. 1959, *J. Aerospace Sci.*, **26**, 16.
Arnaud, K. A., and Fabian, A. C. 1987, preprint.
Auriemma, C., Perola, G. C., Ekers, R., Fanti, R., Lari, C., Jaffe, W. J., and Ulrich, M. H. 1977, *Astr. Ap.*, **57**, 41.
Begelman, M. C. 1986, *Nature*, **322**, 614.
Bicknell, G. V. 1986, *Ap. J.*, **300**, 591.
Burns, J. O., Norman, M. L., and Clarke, D. A. 1987, in *NRAO–Green Bank Workshop 16, Continuum Radio Processes in Clusters of Galaxies*, ed. C. P. O'Dea and J. M. Uson (Greenbank: NRAO), p. 175.
Burns, J. O., O'Dea, C. P., Gregory, S. A., and Balonek, T. J. 1986, *Ap. J.*, **307**, 73.
Canizares, C. R., Fabbiano, G., and Trinchieri, G. 1987, *Ap. J.*, **312**, 503.
Chang, I.-S., and Chow, W. L. 1974, *AIAA J.*, **12**, 1079.
Courant, R., and Friedrichs, K. O. 1948, *Supersonic Flow and Shock Waves* (New York: Interscience), pp. 387–392.
Fabbiano, G., Klein, U., Trinchieri, G., and Wielebinski, R. 1987, *Ap. J.*, **312**, 111.
Fabian, A. C. 1987, in *IAU Symposium 117: Dark Matter in the Universe*, ed. by G. Knapp and J. Kormendy (Dordrecht: Reidel), p. 201.
Fabian, A. C., Nulsen, P. E., and Canizares, C. R. 1984, *Nature*, **310**, 733.
Fanaroff, B. L., and Riley, J. M. 1974, *M.N.R.A.S.*, **167**, 31p.
Forman, W., Jones, C., and Tucker, W. 1985, *Ap. J.*, **293**, 102.
Harlow, F. H. 1964, in *Methods in Computational Physics*, Vol. **3**: *Fundamental Methods in Hydrodynamics*, ed. B. Adler, S. Fernbach, and M. Rotenberg (New York: Academic Press), p. 319.
Ladenburg, R., Van Voorhis, C. C., and Winckler, J. 1949, *Phys. Rev.*, **76**, 662.
Landau, L. D. and Lifshitz, E. M. 1959, *Fluid Mechanics* (Oxford: Pergamon Press).
Lau, J. C. 1981, *J. Fluid Mech.*, **105**, 193.
Livio, M., Soker, N., de Cool, M., and Savonije, G. J. 1986*a*, *M.N.R.A.S.*, **218**, 593.
———. 1986*b*, *M.N.R.A.S.*, **222**, 235.
Miley, G. 1980, *Ann. Rev. Astr. Ap.*, **18**, 165.
Norman, M. L., Smarr, L., and Winkler, K.-H. A. 1985, in *Numerical Astrophysics*, ed. J. M. Centrella, J. M. LeBlanc, and R. L. Bowers (Boston: Jones and Batlett), p. 88.
Nulsen, P. E., Stewart, G. C., and Fabian, A. C. 1984, *M.N.R.A.S.*, **208**, 185.
O'Dea, C. P. 1985, *Ap. J.*, **295**, 80.
O'Dea, C. P., and Baum, S. A. 1987, in *Continuum Radio Processes in Clusters of Galaxies: NRAO–Green Bank Workshop 16*, ed. C. P. O'Dea and J. M. Uson (Greenbank: NRAO), p. 141.
Owen, F. N., Hardee, P. E., and Bignell, R. C. 1980, *Ap. J. (Letters)*, **239**, L11.
Payne, D. G., and Cohn, H. 1985, *Ap. J.*, **291**, 655.
Pedlar, A., Booler, R. V., and Davies, R. D. 1983, *M.N.R.A.S.*, **203**, 667.
Sanders, R. H. 1983, *Ap. J.*, **266**, 73.
Sarazin, C. L. 1986*a*, *Rev. Mod. Phys.*, **58**, 1.
———. 1986*b*, in *Proc. Greenbank Workshop on Gaseous Halos around Galaxies*, ed. by J. Bregman and F. Lockman (Greenbank: NRAO), p. 223.
Sarazin, C. L., and White, R. E., III. 1987, *Ap. J.*, **320**, 32.
Shapiro, A. H. 1953, *The Dynamics and Thermodynamics of Compressible Fluid Flow* (New York: Ronald), pp. 454, 565–566.
Soker, N., and Sarazin, C. L. 1987, in *Proc. NATO Advanced Research Workshop on Cooling Flows in Clusters and Galaxies*, ed. by A. C. Fabian (Dordrecht: Reidel), in press.
Stewart, G. C., Fabian, A. C., Jones, C., and Forman, W. 1984, *Ap. J.*, **285**, 1.
Sumi, D. M., Norman, M. L., Smarr, L. L., and Owen, F. N. 1988, preprint.
Sumi, D. M., and Smarr, L. L. 1984, in *Physics of Energy Transport in Extragalactic Radio Sources: NRAO Workshop 9*, ed. A. H. Bridle and J. A. Eilek (Greenbank: NRAO), p. 168.
Thomas, P. A., Fabian, A. C., and Nulsen, P. E. 1987, *M.N.R.A.S.*, **228**, 973.
Trinchieri, G., and Fabbiano, G. 1985, *Ap. J.*, **296**, 447.
van Breugel, W., Heckman, T., and Miley, G. 1984, *Ap. J.*, **276**, 79.
Walker, R. C., Benson, J. M., and Unwin, S. C. 1987, *Ap. J.*, submitted.
White, R. E., III, and Chevalier, R. A. 1984, *Ap. J.*, **280**, 561.
White, R. E., III, and Sarazin, C. L. 1987*a*, *Ap. J.*, **318**, 612.
———. 1987*b*, *Ap. J.*, **318**, 621.
———. 1987*c*, *Ap. J.*, **318**, 629.
Williams, A. G., and Gull, S. F. 1984, *Nature*, **310**, 33.

CRAIG L. SARAZIN and NOAM SOKER: Department of Astronomy, University of Virginia, P.O. Box 3818 University Station, Charlottesville, VA 22903